Review

Self-assembled perylene diimide based supramolecular heterojunction with Bi$_2$WO$_6$ for efficient visible-light-driven photocatalysis

Kai Zhang[a,b], Jun Wang[a], Wenjun Jiang[a], Wenqing Yao[a,*], Haipeng Yang[b,*], Yongfa Zhu[a,*]

[a] Department of Chemistry, Tsinghua University, Beijing 100084, PR China
[b] College of Materials Science and Engineering, Shenzhen University, Shenzhen City 518060, Guangdong, PR China

ABSTRACT

Bi$_2$WO$_6$ photocatalyst was hybridized with perylene diimide (PDI) via a facile water bath heating method, the composites photocatalytic oxidation of phenol and water decomposition to produce oxygen are simulated under visible light. It was found that the Bi$_2$WO$_6$/PDI composite shows the higher visible light degradation rate towards phenol than self-assembled PDI and Bi$_2$WO$_6$. What's more, it simultaneously exhibits an enhanced oxygen production rate, which is 2 times than that of the pure self-assembled PDI. In the photocatalytic process of Bi$_2$WO$_6$/PDI composites under visible light irradiation, the position of conduction band and valence band between Bi$_2$WO$_6$ and PDI are beneficial to realize photogenerated carriers separation. In this work, we synthesized Bi$_2$WO$_6$/PDI heterojunction which is the same as most of the reported n-n type heterojunction photocatalysts, the CB and the VB levels of one are higher than the corresponding levels of the another semiconductor. A new inorganic and organic composite n-n type heterojunction was form to explain the mechanism of photocatalytic activity enhancement. Self-assembled PDI and Bi$_2$WO$_6$ surface hybridization to promote the separation of photogenerated carriers, electrons in the LUMO orbit of PDI are injected into the conduction band of the Bi$_2$WO$_6$, produced a superoxide radical-based visible light degradation activity.

1. Introduction

Photocatalyst due to the use of solar energy for environmental protection applications have attracted great interest, which can be used for various aspects, such as: air purification, water purification, antifouling dust, antibacterial sterilization. TiO$_2$ photocatalyst has the advantages of low cost, high efficiency and good stability, but its gap width (~3.2 eV) cannot take advantage of the large proportion of visible light in the sunlight and the rapid recombination of photogenerated carriers [1]. The synthesis technology and modified TiO$_2$ to enhanced photocatalytic performance had been reported [2–6]. Not only TiO$_2$, the development of new visible light catalyst has become a hot research.

Bismuth-based compounds (Bi$_2$O$_3$ [7], CaBi$_2$O$_4$ [8], Bi$_2$WO$_6$ [9–11], BiVO$_4$ [12,13], BiPO$_4$ [14], Bi$_2$O$_2$CO$_3$ [15], Bi$_{12}$TiO$_{20}$ [16], Bi$_2$SiO$_5$ [17], BiOX (x = Cl, Br, I)[18]) are made up of the bismuth 6 s and oxygen 2p orbit, with a narrow bandgap that absorbs more sunlight energy. The basic structure of the bismuth-based layered material is that the $(Bi_2O_2)^{2+}$ layer and the various ion layers are alternately stacked with each other, which is favorable for the migration of the photogenerated electron-hole pairs and captured by the inter-layer

water molecules to delay photogenerated carrier recombination, thereby enhancing its photocatalytic activity and becoming a hot topic in the field of photocatalysis. Bi$_2$WO$_6$ has a narrow band gap (~2.8 eV) as an excellent visible light catalyst in bismuth-based compounds.

Compared with inorganic materials, organic materials have many advantages, such as chemical electronic tunability and optical properties, structural diversity, low cost and rich elements of resources. So in the past few decades, organic catalysts have attracted many researchers to conduct related research. However, organic catalysts are mainly based on two organic materials: (1) Organometallic complexes [19], but metal complexes may limit their practical application due to the high cost, potential toxicity and bad sustainability; (2) Covalent organic polymers, including commonly reported carbon nitrides [20], triazine/hydrazone-based carbon nitrides [21], some covalent organic polymers based on poly(azomethine) [22] and so on. The development of organic materials for visible light driven photocatalysis is considered to be one of the most promising way to solve environmental and solar energy use issues. Molecule self-assembly has been used to tailor surface properties [23], non-covalent self-assembled supramolecular system composed of pure organic molecules alone as a photocatalyst with wide visible light response has been reported recently. PDI molecules

photocatalyst are self-assembled by the formation of one-dimensional supramolecular organic nanomaterials which can be used as organic pollutants degradation and visible light oxidation of water, it is a special n-type organic semiconductor material which exhibits excellent thermal/light stability, high electron affinity and charge carrier mobility [24–28].

It is one of the effective ways to improve the photocatalytic performance by constructing heterojunction structure through two different semiconductor catalyst materials [29]. In heterostructure, band structures are pivotal to determine the photoabsorption, charge separation efficiency, photooxidation or reduction capacity of the whole system. It has been confirmed that compare with n-n heterojunction, there is a poor concentration of carriers on both sides of p-n heterojunction interface and form built-in electric field beneficial to separate carriers. There has few report about n-n heterojunction, for example $CeO_2/g-C_3N_4$ [30]. In this work, we use n-type inorganic and organic semiconductor materials to form n-n heterojunction, and then explain the mechanism of enhanced photocatalytic degradation. Both Bi_2WO_6 and PDI have their own composite materials, such as: Bi_2WO_6/C_3N_4 [31,32], $CQDs/Bi_2WO_6$ [33], 3D-3D Bi_2WO_6/graphene hydrogel [34], Bi_2WO_6/Bi_2S_3 [35], PDI-Pt/TiO$_2$ [36], PDI/g-C$_3$N$_4$ [37], PDI/copper phthalocyanine [38], TCNQ-PTCDI [39] and PTCDI/P25 TiO$_2$ [40], but PDI and bismuth heterostructured composite semiconductor materials have not been reported so far. The position of valence band and conduction band between Bi_2WO_6 and PDI are conducive to the formation of heterojunction, thereby promoting the separation of photogenerated electrons and holes to improve its catalytic performance. For the n-n type heterojunction, due to the presence of a large number of electron traps in the interface state, it can capture the conduction band electrons on both sides of the interface, leaving the interface negatively charged. In order to satisfy the neutral condition, a positively charged depletion layer must be formed on both sides of the interface, resulting in the bending of the depletion layer on both sides of the interface upward to form a built-in electric field, which promote the movement of electrons. Moreover, the absorption side of Bi_2WO_6/PDI composite material has little red shift increased visible light absorption. Compared to traditional inorganic semiconductor composites, the diversity of organic composite semiconductor materials is conducive to the expansion of the field. In this work, the composite materials were prepared by the one-step water bath heating method, so that the PDI molecules were combined with Bi_2WO_6 in the water bath self-assembled process to improve the photocatalytic degradation activity.

2. Experimental section

2.1. Synthesis of Bi_2WO_6/Self-assembled PDI composites

Bi_2WO_6 nanocatalyst was prepared by low temperature hydrothermal method. The specific preparation process was as follows: 0.005 mol $Bi(NO_3)_3·5H_2O$ and 0.0025 mol $Na_2WO_4·2H_2O$ were placed in a beaker, 30 ml deionized water was added and the mixture was sonicated for 10 minutes to obtain a precursor in a hydrothermal autoclave within 24 hours of water heat process at 180 °C. The product was cooled then rinsed and centrifuged with deionized water following dried at 60 °C.

Synthesis of PDI: 1.376 g (3.507 mmol) of perylene-3,4,9,10-tetracarboxylic dianhydride, 2.5 g (28.06 mmol) of 3-aminopropionic acid and 18 g of imidazole were placed in a three-necked flask to heat at 100 °C for 4 hours under the protection of argon. The reaction mixture was cooled to room temperature and dispersed in 100 mL ethanol, followed by the addition of 300 mL 2 M HCl and the mixture was stirred overnight. The resulting red solid was collected by filtration through a 0.45 μm membrane filter and washed with distilled water thoroughly until the pH of the wash solution became neutral. The collected solid was dried at 60 °C in oven.

Self-assembled of PDI: A stock solution of 200.0 mL N, N'-bis (propionic acid) -phenyl-3,4,9,10-tetracarboxylic acid diimide (5.0 mM) was prepared and added 834 μL triethylamine solution with constantly stirring, the solution becomes red. Followed by the addition of 27.3 mL 4.0 M HNO_3 to form PDI nanofibers. Washed with distilled water thoroughly until the pH of the product became neutral, and the collected solid was dried at 60 °C.

Preparation of Bi_2WO_6/PDI Composites: A stock solution of 200.0 mL N, N'-bis (propionic acid)-perylene-3,4,9,10-tetracarboxylic acid diimide (5.0 mM) was prepared and added 834 μL triethylamine solution and keep stirring, the solution becomes red. Take 187.27 mL stock solution (containing PDI 500 mg) to add different quality ratio of Bi_2WO_6 catalyst stirring 30 minutes and then ultrasound 15 minutes. Followed by heating in a water bath at 60 °C and adding 25.56 ml 4 M HNO_3 strring for 1 hour. The product was centrifuged to neutral and dried at 60 °C

2.2. Characterization of materials

The scanning electron microscopy (FE-SEM, Hitachi SU-8010) and the transmission electron microscope (TEM, equipped with Hitachi HT7700 electron microscope, the accelerating voltage of 100 kV) were used to observe the morphology of the material; The high-resolution transmission electron microscopy (HRTEM, JEM 2010 F) at the accelerating voltage of 200 kV, the lattice plane stripe of Bi_2WO_6/PDI and elemental analysis were obtained; UV–vis diffuse reflection spectra (DRS) were obtained on a Hitachi U-3010 UV–vis spectrophotometer, $BaSO_4$ was used as the reflectance stan-dard in the experiment; X-ray diffractometer(Cu Kα, λ = 1.5406 Å, 40 kV, 40 mA) of the recording material at a scanning rate of 5° min^{-1}, 2θ ranges from 5° to 80° to get X-ray diffraction (XRD) pattern; The scanning rate (FT-IR) spectra of the material were measured by a Bruker V70 spectrometer in the frequency range of 600 cm^{-1} to 2000 cm^{-1} with a resolution of 4 cm^{-1}. Fluorescence spectrometer (using 468 nm excitation wavelength); Electrochemical workstations (CHI-660E, China) is used to measure the photocurrent response and electrochemical impedance; The JES-FA200 EPR Spectrometer paramagnetic resonance spectrometer was used to detect the active species, containing spin-trapping probes such as 5,5-dimethyl-1-pirroline-N-oxide (DMPO). Visible light was obtained from a 500 W xenon lamp (Institute for Electric Light Sources, Beijing) with a 420 nm cutoff filter.

2.3. Evaluation of visible light photocatalytic activity

The photocatalytic activity of the prepared material was evaluated by the degradation of the phenol solution. The 500 W xenon lamp was used as a light source in the evaluation of catalytic activity with an average light intensity of 28 mW/cm^2. The cut filter (> 420 nm) was used and the concentration of the phenol solution was 5 ppm.

The photodegradation reaction was carried out in a quartz tube reactor using 50 mL 5 ppm phenol solution and 25 mg photocatalyst powder. The visible light source is obtained by a 500 W xenon lamp with a cutoff filter (> 420 nm). The suspension solution was ultrasonically dispersed in the dark for 15 minutes before irradiation and then magnetically stirred for 1 hour to achieve adsorption-desorption equilibrium. Every half an hour, the 2.5 mL solution was centrifuged to remove the photocatalyst. The upper suspension was filtered with a microporous membrane (0.45 μm in diameter) to protect the column. The concentration of phenol was characterized by a high performance liquid chromatography (HPLC) system. The mobile phase used for the elution of phenol and its degradation from the HPLC column consisted of methanol and water (55:45 by volume). The elution time was 5 minutes and the flow rate was 1 mL/min. The detection wavelength was 270 nm and chromatographic column was a Venusil XBP-C18 (3.9 × 200, Agela Technologies Inc.) column.

The photocatalyst powders (50 mg) were dispersed by a mag-netic stirrer in 100 mL of $AgNO_3$ (aq) in a reaction cell. The visible light

source was obtained by a 300 W xenon lamp with cutoff filter (> 420 nm). The amount of evolved oxygen was determined using a gas chromatograph.

2.4. Electrochemical measurement

The photocurrent and electrochemical impedance spectroscopy (EIS) of Bi_2WO_6/PDI composites were performed on an electrochemical workstation (CHI-660E, China) using a standard three-electrode electrochemical system under simulated visible light irradiation. ITO deposited with photocatalyst as working electrode, platinum wire and saturated calomel were used as counter electrode and reference electrode respectively, and Na_2SO_4 solution (0.1 M) was used as electrolyte solution.

ITO/Bi_2WO_6/PDI was prepared by dip coating: 5 mg Bi_2WO_6/PDI photocatalyst was suspended in 0.75 mL ethanol to prepare a slurry which was coated onto a 2 cm × 4 cm indium-tin oxide (ITO) glass electrode. The prepared electrode was calcined at 120 °C for 2 hours and then slowly cooled to room temperature. The photoelectric response of the sample was measured at 0.0 V and the electrochemical impedance spectroscopy (EIS) was carried out at an open circuit potential at a frequency of 0.01–10,000 Hz. ITO/Bi_2WO_6 and ITO/PDI were compared under the same conditions.

3. Results and discussion

3.1. Structure and morphology Characterization

XRD is usually used to determine the crystal type and crystallinity of the material. The composition, atom or molecular structure of the material are obtained from the diffraction pattern. It can be seen from the XRD spectrum of Fig. 1a that Bi_2WO_6 has good crystallinity. All the composite samples exhibited the distinctive peaks at $2\theta = 28.26°$, 32.98°, 47.18°, 55.84° and 58.44°, which can be indexed orthorhombic phase Bi_2WO_6 (JCPDS:39-0256). Self-assembled PDI organic molecules have poor crystallinity and have more diffraction peaks in the range of 5–28°. The upper right corner of Fig. 1a is the XRD diffraction pattern in the range of 5–28° containing self-assembled PDI. It can be seen that the self-assembled PDI diffraction peak of Bi_2WO_6/PDI composites enhanced with the increase of self-assembled PDI mass percentage, both PDI or Bi_2WO_6 crystal structure will not affect each other. Fig. 1b shows the FTIR spectra of a series of samples. The pure Bi_2WO_6 sample is mainly absorbed at 400–800 cm^{-1} and belongs to Bi−O stretching and W−O−W bridging stretching mode. With the increase content of Bi_2WO_6 in Bi_2WO_6/PDI composites, the absorption peak at 698 cm^{-1} is more obvious. But compared with pure Bi_2WO_6, the peak at 698 cm^{-1} shows apparent blue shift indicate the force between Bi_2WO_6 and self-assembled PDI. Self-assembled PDI as organic material, which is shown at 1688 cm^{-1} C=O and 1652 cm^{-1} C=C stretching, may indicate the carboxyl and benzene ring structure. The FTIR spectra show that the structures of self-assembled PDI and Bi_2WO_6 have not changed in Bi_2WO_6/PDI composites.

The FE-SEM images of microstructure and morphology of Bi_2WO_6, self-assembled PDI and Bi_2WO_6/PDI composite can be seen in Fig. S1. Self-assembled PDI is a clustered nanorod-like morphology shown in Fig. S1b, figure S1a show a pure Bi_2WO_6 was nanosheet structure and from Fig. S1c it can be seen that Bi_2WO_6 nanosheets were successfully attached to the self-assembled PDI surface. Its internal structure is further observed by TEM images. Fig. 2 shows the TEM morphology of Bi_2WO_6, PDI and 50%-Bi_2WO_6/PDI composite respectively. The Bi_2WO_6 nanosheet in Fig. 2b is about 50–100 nm in size, and it can be seen in Fig. 2d that the inner structure is further observed by HR-TEM image. It can also be seen that the lattice spacing of 0.315 nm corresponds to the (131) plane of Bi_2WO_6, and the dark part is self-assembled PDI nanorod structure can be seen at its edge, indicating that Bi_2WO_6 and PDI surface pass through a certain force together. The self-
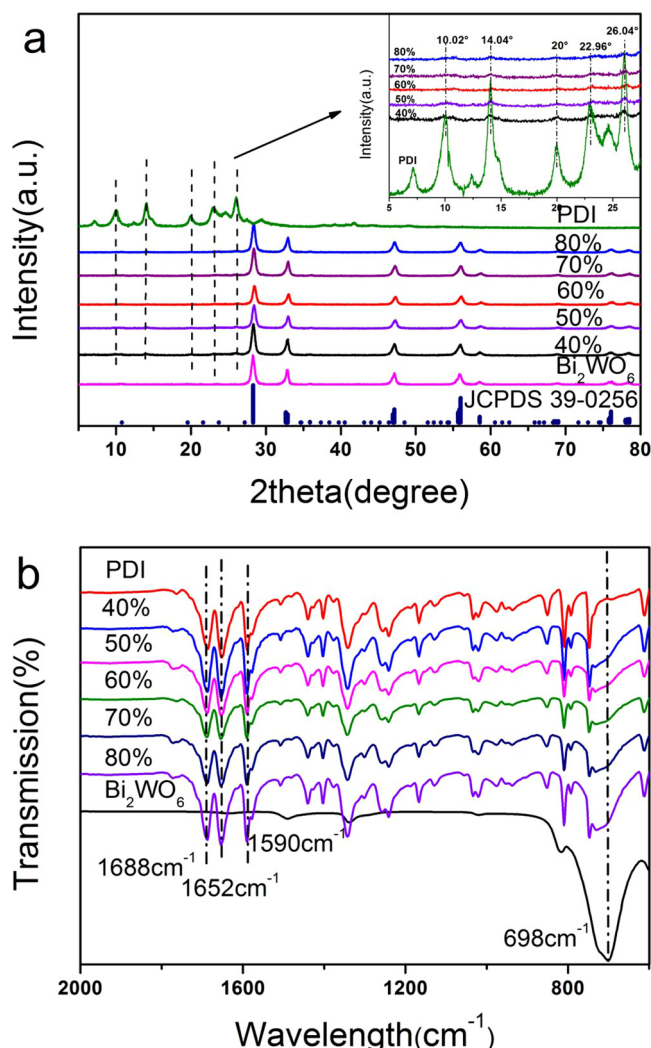

Fig. 1. A series of samples (a) XRD spectra; (b) FTIR spectra.

assembled PDI molecules in Fig. 2a exhibit a nanorod-like structure with a diameter of about 50 nm, Fig. 2c shows that a small amount of Bi_2WO_6 nanosheet is loaded on a self-assembled PDI nanorods. The molecular structure model of Bi_2WO_6/PDI shown in Fig. S2. The EDS element analysis of 50%-Bi_2WO_6/PDI composite is shown in Fig. S3, and the middle of the bright contrastis were Bi_2WO_6 nanosheets. It can also be seen by EDS mapping that there are more Bi, W and O elements in the middle, while the surrounding dark contrast for the self-assembled PDI nanorods with the composition of elements C, N, O. From the FE-SEM and TEM images, it's obviously observed Bi_2WO_6/PDI composites were successfully prepared.

Fig. 3 shows the UV–vis diffuse reflection spectra (DRS) of Bi_2WO_6, self-assembled PDI and 50%-Bi_2WO_6/PDI photocatalyst. It is clear that the pure Bi_2WO_6 has few visible light absorption. The absorption edge of pure Bi_2WO_6 is about 443 nm, indicating that photocatalytic degradation ability is attributed to the absorption from 420 to 443 nm under visible light. After hybrid with self-assembled PDI, the absorption wavelength of composite is expanded to 729 nm which display a better visible light respond. Compared with pure self-assembled PDI, it shows a little enhanced visible light absorption. The bandgap width is calculated according to the formula: $Eg = 1240/\lambda g$ (eV), and the bandgap width of Bi_2WO_6 and PDI are about 2.79 eV and 1.71 eV.

3.2. Enhancement of photocatalytic activity

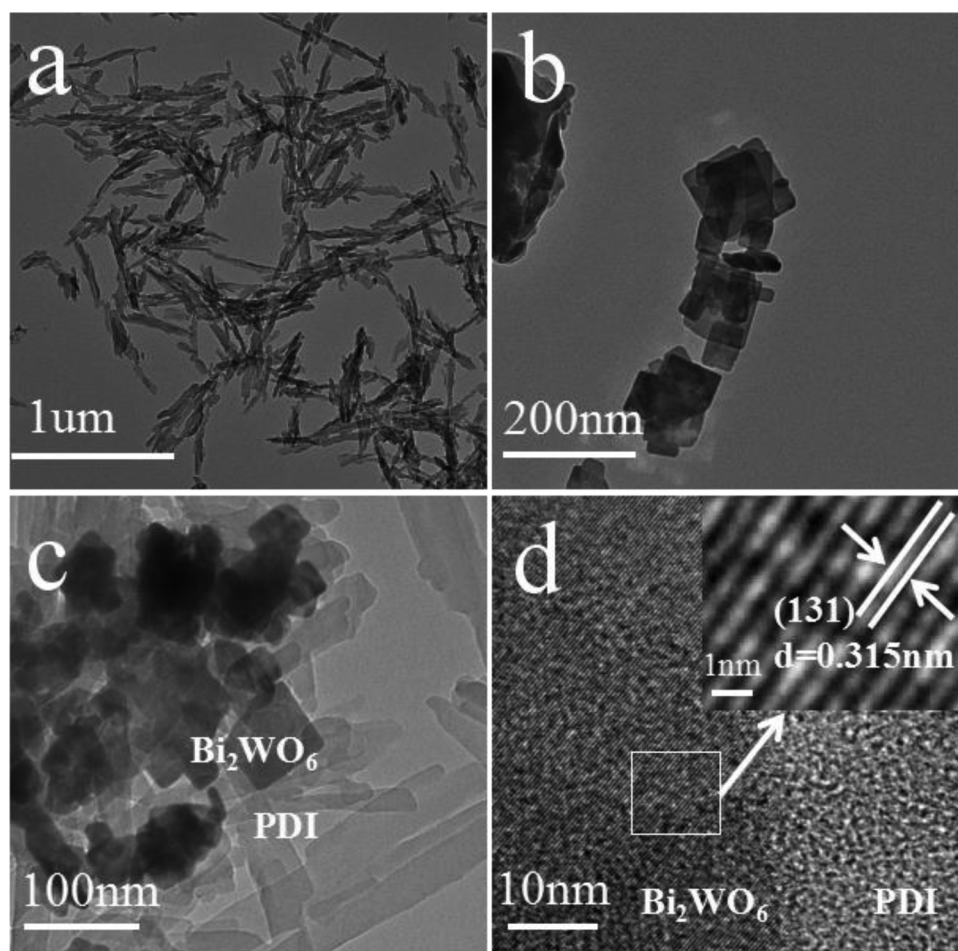The photocatalytic activity of the prepared samples were evaluated

Fig. 2. TEM images of (a) self-assembled PDI; (b) Bi_2WO_6; (c) 50%-Bi_2WO_6/PDI (d) HR-TEM image of 50%-Bi_2WO_6/PDI sample.
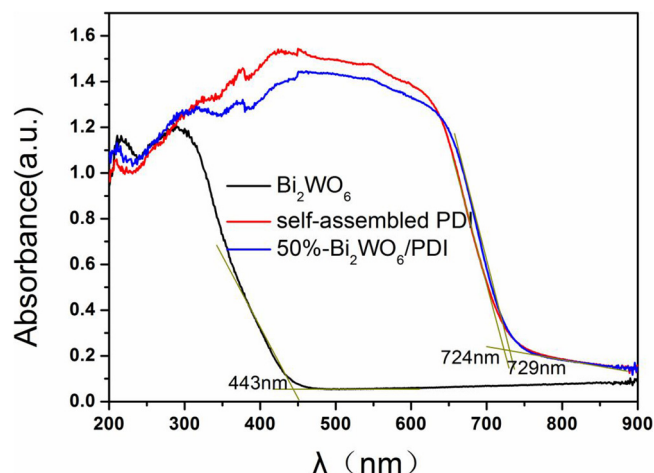

Fig. 3. The UV–vis diffuse reflection spectra (DRS) of Bi_2WO_6, self-assembled PDI and 50%-Bi_2WO_6/PDI photocatalyst.

by the degradation of phenol and water oxidation. Fig. 4a shows the concentration change of phenol under visible light ($\lambda > 420$ nm) with different catalysts, the apparent rate constants (k)-photocatalytic degradation of phenol was calculation shown in 4b Bi_2WO_6 and self-assembled PDI composite samples were recorded as 40%, 50%, 60%, 70% and 80% by mass ratio of m(Bi_2WO_6):m(PDI). It can be seen from the figure that when the mass ratio of m(Bi_2WO_6):m(PDI) = 50%, the sample has the highest visible photocatalytic activity. And the physical mixing sample of Bi_2WO_6/PDI show lower activity than pure self-

assembled PDI, which mean Bi_2WO_6 and PDI successful compound together by water bath heating method. The degradation process is suitable for the pseudo-first order kinetics, and the rate constant k is equal to the corresponding slope of the fitting line. The photocatalytic activity of Bi_2WO_6 under simulated light was lower than others and the apparent rate constant k = 0.0413 h^{-1}. While the pretreatment of PDI degradation of phenol activity is better, the apparent rate constant k = 0.0887 h^{-1}. The catalytic activity of Bi_2WO_6/PDI composites prepared by one-step ultrasonic-water bath heating were improved, and the catalytic activity reached the maximum value of k = 0.357 h^{-1} when m (Bi_2WO_6):m(PDI) = 50%, it was about 7.65 times higher than Bi_2WO_6 and 1.75 times than that of self-assembled PDI molecule k = 0.204 h^{-1}, which indicated that Bi_2WO_6 combined with self-assembled PDI molecule to enhance the catalytic activity. Further increasing the m(Bi_2WO_6):m(PDI) ratio, we can see that the activity decreased slightly, it probably due to Bi_2WO_6 and PDI reached a more complex area or Bi_2WO_6 content increased easy reunited together to reduce its utilization. Fig. 4c is a three-cycle test of 50%-Bi_2WO_6/PDI catalyst degradation of phenol. At the second cycle, the activity decreased by about 10% and then remained stable which due to loss of the first fraction of the catalyst. Three cycles of activity remained stable, indicating that the catalyst can be efficiently recycled. The results (Fig. S4a and S4b) were determined by HPLC for the presence of phenol in simulated visible light ($\lambda > 420$ nm) irradiation. A typical HPLC chromatogram of self-assembled PDI and 50%-Bi_2WO_6/PDI was recorded by an ultraviolet-visible detector. Peak 1 corresponds to phenol, peak 2 corresponds to a small part of the self-assembled PDI organic molecules dissolution is not completely separated from the solution, no other intermediate products, indicating that self-assembled PDI and its
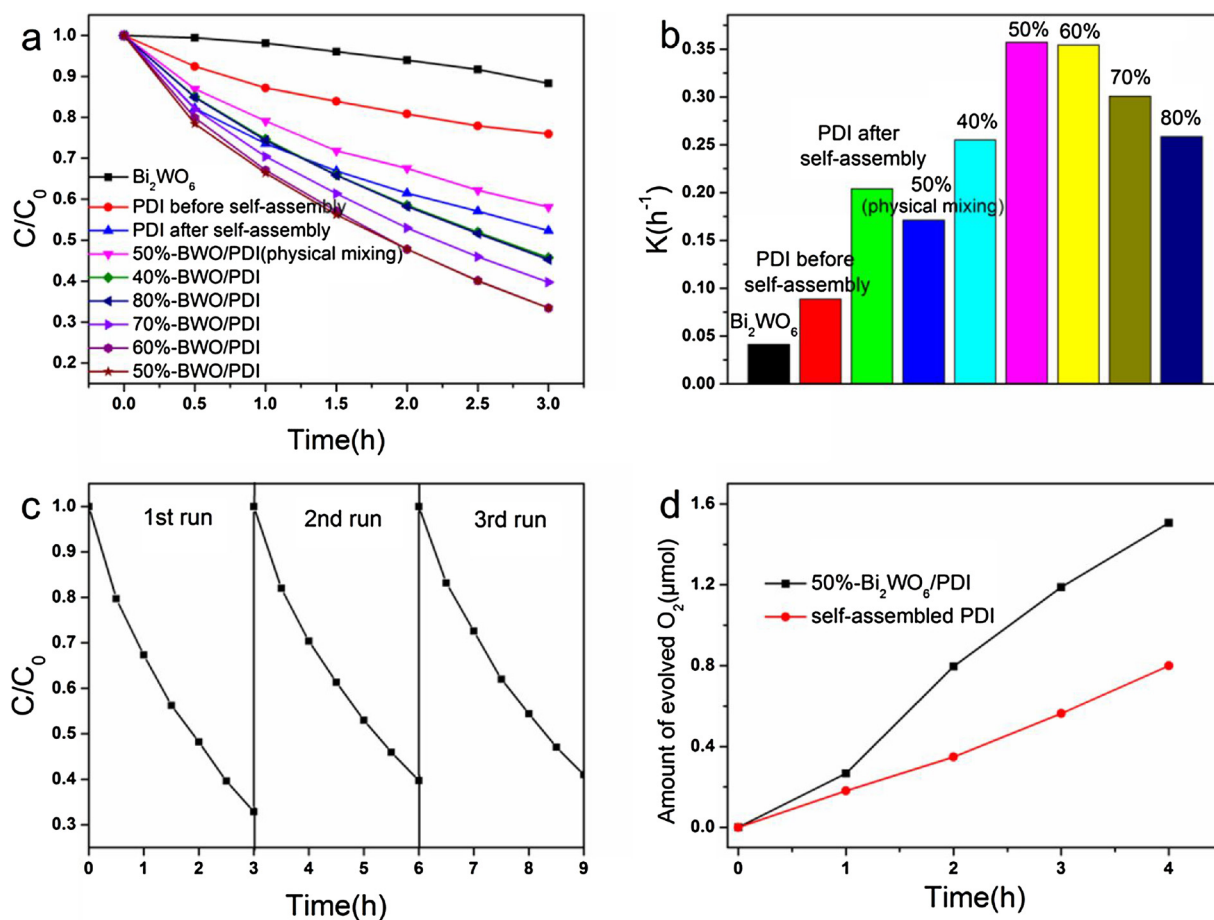
Fig. 4. (a) Photocatalytic degradation of 5 ppm phenol under visible light (λ > 420 nm); (b) degradation rate constant (k); (c) 50%-Bi_2WO_6/PDI cycle degradation of phenol performance test; (d) Oxygen evolution from water by PDI and 50%-Bi_2WO_6/PDI sample in the presence of an electron acceptor (10 mM silver nitrate).

composite material 50%-Bi_2WO_6/PDI can be effective mineralization of phenol. The strong photooxidative ability of catalyst can be further certified by the water oxidation experiments. The photocatalytic oxygen evolution tests were carried out under visible light (λ > 420 nm) irradiation. Silver nitrate solution (0.01 M) was elected as an electron acceptor, 50 mg photocatalyst scattered in 100 mL silver nitrate solution, 50%-Bi_2WO_6/PDI exhibits a better photooxidative ability which was about 2 times than that of pure self-assembled PDI, it also means enhanced carrier separation efficiency. Further discussion on effects of the different mass of self-assembled PDI shown in Fig. S5. Because using 25 mg catalyst as a standard comparison, 13.9, 14.7, 15.6, 16.7, 17.9 mg PDI are corresponds to different mass ratio 80%–40% Bi2WO6/PDI. Fig. S5a shows the concentration change of phenol under visible light (λ > 420 nm) with different mass of self-assembled PDI. It can be seen that the degradation rate constant (k) was increased with more self-assembled PDI added in Fig. S5b. This is due to the increased concentration of catalyst in solution. It also reflects the mass of self-assembled PDI have influence on photocatalytic activity but not the major factor, because 40%-Bi_2WO_6/PDI has the most mass of self-assembled PDI but not the best photocatalytic activity. Compared with Fig. 4b, we can see that as the mass proportion of Bi_2WO_6 increases by 40%–80% (that is, the mass proportion of PDI decreases), it shows the trend of increase and followed by a drop. And 50%-Bi_2WO_6/PDI which contains about 16.7 mg PDI/25 mg catalyst has the best photocatalytic activity.

3.3. Visible light catalytic activity enhancement mechanism

The mechanism of enhanced photocatalytic activity of Bi_2WO_6/PDI

composite was further studied by photoelectrochemistry process. Organic pollutants in the photocatalytic decomposition process, the separation of photogenerated electrons and holes plays a very important role, which can be evaluated by typical photocurrent and electrochemical impedance spectroscopy (EIS). The transient photocurrent response of Bi_2WO_6, self-assembled PDI, 50%-Bi_2WO_6/PDI composite and the corresponding electrochemical impedance (EIS) Nyquist diagram shown in Fig. 5 Transient photocurrent of all samples is very stable in the cycle. Under the visible light (λ > 420 nm) irradiation, the pure Bi_2WO_6 has a very weak light current response of only 0.025 μA cm^{-1}, self-assembled PDI photocurrent response is slightly higher, about twice than the Bi_2WO_6, 50%-Bi_2WO_6/PDI composite has the largest photocurrent response, the stable photocurrent is about 0.1 μA cm^{-1} which higher than Bi_2WO_6 and self-assembled PDI, it show rapid increase in current when the light on but followed by a drop, the enhanced photocurrent response shows that the separation efficiency of photogenerated carriers and the photocatalytic performance are improved. It was found that the photocurrent of Bi_2WO_6/PDI composite is decreases with time, which is due to the photogenerated electrons easily ran to the surface, resulting in a loss of surface recombination current. Fig. 5b shows the EIS Nyquist plot of Bi_2WO_6, self-assembled PDI and 50%-Bi_2WO_6/PDI. The radius of the arc on the EIS spectrum reflects the solid interface delamination resistance and the surface charge transfer resistance. The smaller radius of the arc on the EIS Nyquist diagram indicates that the separation of photogenerated electrons and holes is more. Under the conditions of visible light (λ > 420 nm) irradiation, the radius of the arc on the EIS spectrum of Bi_2WO_6, self-assembled PDI and 50%-Bi_2WO_6/PDI composite were reduced than non-light, indicating that the photogenerated photons were
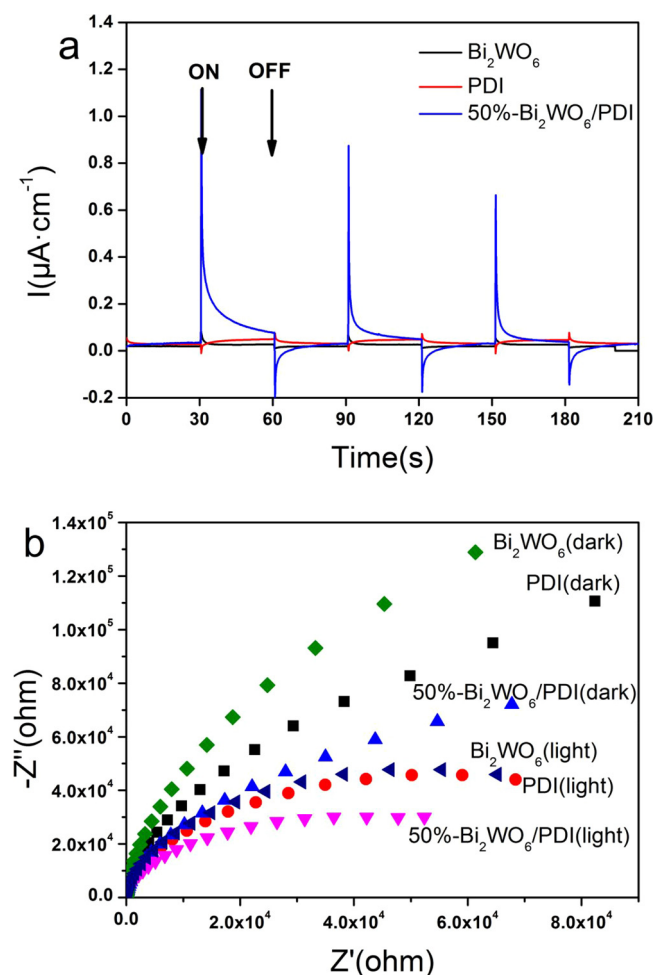
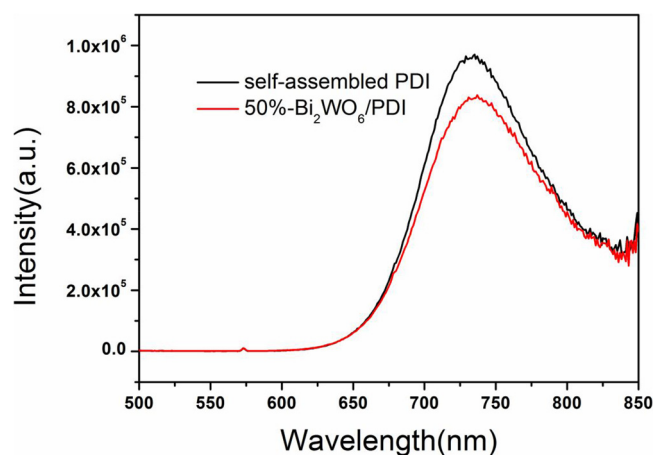**Fig. 5.** Bi$_2$WO$_6$, PDI and 50%-Bi$_2$WO$_6$/PDI films (a) Photocurrent response; (b) EIS spectra.

Fig. 6. Photoluminescence spectra of self-assembled PDI, 50%-Bi$_2$WO$_6$/PDI photocatalyst.

produced. And 50%-Bi$_2$WO$_6$/PDI composite has the smallest arc radius under visible light conditions, indicating that it is more separation of the photo-generated electrons and holes than pure Bi$_2$WO$_6$ and self-assembled PDI, thus increasing composite visible light photocatalytic activity (Fig. 6).

The photoluminescence spectra of self-assembled PDI, 50%-Bi$_2$WO$_6$/PDI at excitation wavelength of 468 nm, the pure self-assembled PDI performance is show stronger peak. The PL signal of
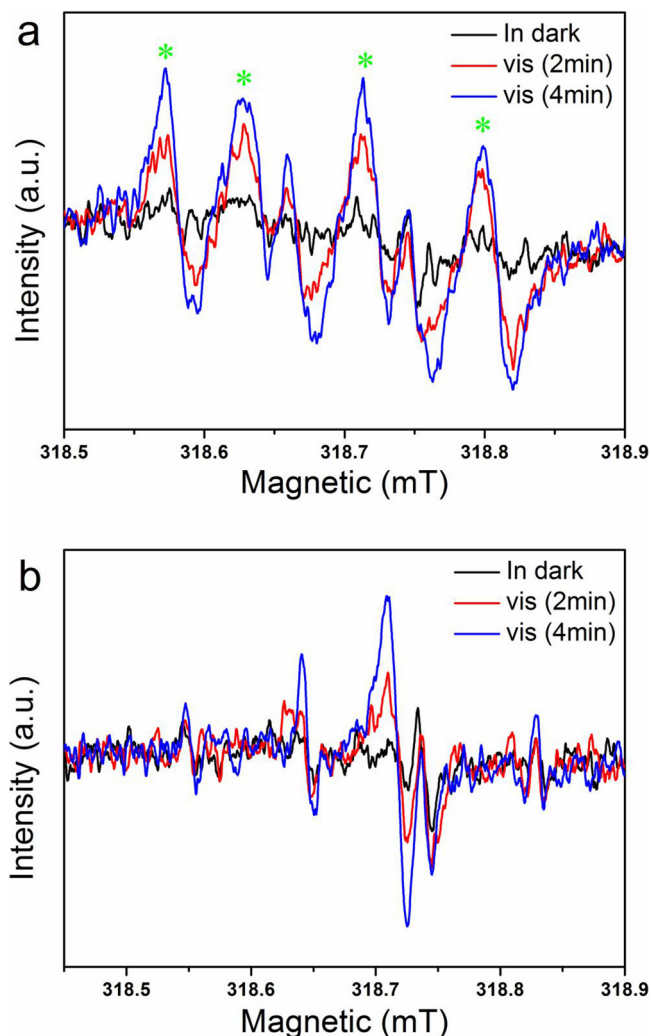

Fig. 7. 50%-Bi$_2$WO$_6$/PDI material without light conditions and visible light (λ > 420 nm) electron spin resonance (ESR) spectra of radical adducts trapped by DMPO; (a) DMPO-superoxide radical (·O$_2^-$) species detected for the sample dispersion in methanol; (b) DMPO-hydroxyl radical (·OH) species detected for the sample dispersion in water.

Bi$_2$WO$_6$/PDI composite is weakened than pure self-assembled PDI indicating that the recombination of photogenerated electrons and holes is significantly reduced. Compared with pure self-assembled PDI, the PL signal of Bi$_2$WO$_6$/PDI is clearly redshift, indicating some interaction between Bi$_2$WO$_6$ and PDI interface. Therefore, Bi$_2$WO$_6$ and PDI successfully compound enhanced the efficiency of photo-generated electrons and holes, and further confirmed that Bi$_2$WO$_6$/PDI composites enhanced photocatalytic activity.

Electron spin resonance (ESR) tests were carried out to further reveal the specific active species of Bi$_2$WO$_6$/PDI composite in the photocatalytic degradation reaction. Fig. 7 shows the signal responses of (a) the superoxide radical (·O$_2^-$); (b) hydroxyl radical (·OH) both detected by the ESR spectrometer. DMPO (5,5-dimethyl-1-pyrroline N-oxide) is a spin trap can obvious reflection of ·O$_2$- or ·OH. It can be seen that ·O$_2$- has a strong signal response but ·OH signal is very weak under visible light irradiation that indicating Bi$_2$WO$_6$/PDI composite materials in the photocatalytic degradation of the active species is mainly superoxide radical (·O$_2^-$).

On the basis of the above analysis, a possible mechanism for the oxidation of phenol and water decomposition to produce oxygen over Bi$_2$WO$_6$/PDI heterojunction photocatalyst under visible irradiation is proposed as shown in Scheme 1. Photogenerated electrons and holes are generated on both Bi$_2$WO$_6$ and PDI under visible light irradiation.
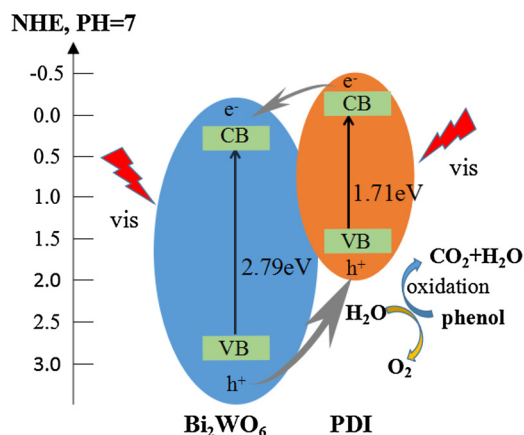
Scheme 1. Schematic diagram of electron-hole pair separation and the possible reaction mechanism of Bi_2WO_6/PDI composite materials under visible light (λ > 420 nm).

The CB of Bi_2WO_6 is lower than that of self-assembled PDI, so the photogenerated electrons can be injected easily from self-assembled PDI to Bi_2WO_6, and form a built-in electric field is beneficial to the separation of electrons. The holes on the VB of self-assembled PDI shows strong oxide capability, electrons in the LUMO orbit of PDI are injected into the conduction band of the Bi_2WO_6, produced superoxide radical ($\cdot O_2^-$) which contributes to the enhancement on phenol degradation activity and water decomposition to produce oxygen ability of Bi_2WO_6/PDI heterojunction photocatalyst under visible light.

4. Conclusion

In this work, Bi_2WO_6/PDI composites were prepared by a water bath heating method. Compared with pure Bi_2WO_6 and self-assembled PDI, Bi_2WO_6/PDI have excellent visible photocatalytic degradation and oxygen production performance, which is beneficial to oxidative and degradation of organic pollutants. In the Bi_2WO_6/PDI composite photocatalyst, the contact surface of the Bi_2WO_6/PDI composite photocatalyst forms a n-n type heterojunction structure. Self-assembled PDI and Bi_2WO_6 surface hybridization to promote the separation of photogenerated carriers, electrons in the LUMO orbit of PDI are injected into the conduction band of the Bi_2WO_6, produced a superoxide radical-based visible light degradation activity.

Acknowledgements

Appendix A. Supplementary data

Supplementary material related to this article can be found, in the online version, at doi:https://doi.org/10.1016/j.apcatb.2018.03.059.

References

[1] A. Fujishima, Nature 238 (1972) 37–38.
[2] F. Cao, Y. Li, C. Tang, Res. Chem. Intermed. 42 (2016) 5975–5981.
[3] Z. Bian, J. Zhu, H. Li, J. Photoch. Photobio. C 28 (2016) 72–86.
[4] C. Tang, L. Liu, Y. Li, Appl. Catal. B 201 (2017) 41–47.
[5] Y. Li, Y. Bian, H. Qin, Appl. Catal. B 206 (2017) 293–299.
[6] H. Qin, Y. Bian, Y. Zhang, Chin. J. Chem. 35 (2017) 203–208.
[7] L. Zhou, W. Wang, H. Xu, Chemistry 15 (2009) 1776–1782.
[8] J. Tang, Z. Zou, J. Ye, Angew. Chem. Int. Ed. 43 (2004) 4463–4466.
[9] C. Zhang, Y. Zhu, Chem. Mater. 17 (2005) 3537–3545.
[10] F. Amano, A. Yamakata, B. Ohtani, J. Am. Chem. Soc. 130 (2008) 17650–17651.
[11] L. Zhang, Y. Wang, H. Cheng, Adv. Mater. 40 (2010) 1286–1290.
[12] K. Akihiko, O. Keiko, K. Hideki, J. Am. Chem. Soc. 121 (1999) 11459–11467.
[13] R. Li, F. Zhang, D. Wang, Nat. Commun. 4 (2013) 1432.
[14] C. Pan, Y. Zhu, Environ. Sci. Technol. 44 (2010) 5570–5574.
[15] H. Cheng, B. Huang, K. Yang, ChemPhysChem 11 (2010) 2167–2173.
[16] W. Wei, Y. Dai, B. Huang, J. Phys. Chem. C. 113 (2009) 5658–5663.
[17] R. Chen, J. Bi, L. Wu, Inorg. Chem. 48 (2009) 9072–9076.
[18] X. Zhang, Z. Ai, F. Jia, J. Phys. Chem. C. 112 (2008) 747–753.
[19] T. Hiroyuki, K. Kazuhide, I. Haruo, I. Osamu, J. Am. Chem. Soc. 130 (2008) 2023–2031.
[20] X. Wang, K. Maeda, A. Thomas, K. Takanabe, G. Xin, J.M. Carlsson, K. Domen, M. Antonietti, Nat. Mater. 8 (2009) 76.
[21] K. Schwinghammer, B. Tuffy, M.B. Mesch, E. Wirnhier, C. Martineau, F. Taulelle, W. Schnick, J. Senker, B.V. Lotsch, Angew. Chem. Int. Ed. 125 (2013) 2495–2499.
[22] M.G. Schwab, M. Hamburger, X. Feng, J. Shu, H.W. Spiess, X. Wang, M. Antonietti, K. Müllen, Chem. Commun. 46 (2010) 8932.
[23] M.A. Frank, C. Meltzer, B. Braunschweig, Appl. Surf. Sci. 404 (2017) 326–333.
[24] A. Datar, K. Balakrishnan, L. Zang, Chem. Commun. 49 (2013) 6894–6896.
[25] C. Shuai, P. Slattum, C. Wang, Chem. Rev. 115 (2015) 11967–11998.
[26] D. Liu, J. Wang, X. Bai, Adv. Mater. 28 (2016) 7284–7290.
[27] J. Wang, W. Shi, D. Liu, Appl. Catal. B 202 (2017) 289–297.
[28] L. Zeng, T. Liu, C. He, J. Am. Chem. Soc. 138 (2016) 3958–3961.
[29] J. Low, J. Yu, M. Jaroniec, Adv. Mater. 29 (2017) 1601694.
[30] N. Tian, H. Huang, C. Liu, J. Mater. Chem. A 3 (2015) 17120–17129.
[31] Y. Wang, X. Bai, C. Pan, J. Mater. Chem. 22 (2012) 11568–11573.
[32] J. Wang, L. Tang, G. Zeng, Appl. Catal. B 209 (2017) 285–294.
[33] X. Qian, D. Yue, Y. Zhao, Appl. Catal. B 193 (2016) 16–21.
[34] J. Yang, D. Chen, Y. Zhu, Appl. Catal. B 205 (2017) 228–237.
[35] L. Yan, Y. Wang, H. Shen, Appl. Surf. Sci. 393 (2017) 496–503.
[36] S. Chen, Y. Li, C. Wang, Rsc Adv. 5 (2015) 15880–15885.
[37] S. Chen, C. Wang, B. Bunes, Appl. Catal. A 498 (2015) 63–68.
[38] H. Wang, L. Zhao, X. Liu, Dyes Pigments 137 (2017) 322–328.
[39] Z. Zhang, J. Wang, L. Di, Acs Appl. Mater. Interfaces 8 (2016) 30225–30231.
[40] W. Wei, D. Liu, Z. Wei, ACS Catal. 7 (2017) 652–663.